ACS Electrochemistry

pubs.acs.org/electrochem

Article

Nitrogen Electrochemical Reduction Reaction Pathways Evidenced by Online Electrochemical Mass Spectrometry and Isotope Labeling on the MoS_2 Surface

Rodrigo Gomes de Araujo and Joelma Perez*

Cite This: ACS Electrochem. 2025, 1, 294−302

Read Online

ACCESS | Metrics & More | Article Recommendations | Supporting Information

ABSTRACT: The electrochemical nitrogen reduction reaction (NRR) for ammonia production is a promising method for mitigating CO_2 emissions. In this study, we investigate the NRR in alkaline media using both labeled and unlabeled compounds on MoS_2 electrodes, employing online electrochemical mass spectrometry (OLEMS) and UV-vis spectroscopy to identify gaseous and solution-phase products, respectively. Notably, OLEMS results reveal the detection of N_2H^+ and $N_2H_2^+$ species as intermediates of the NRR, following the observation of N_2 consumption at −0.4 V vs. RHE and the onset of NH_3 production around −0.5 V vs. RHE. However, $N_2H_3^+$ and $N_2H_4^+$ species were not observed. UV-vis spectroscopy confirmed the production of NH_3. The N_2 molecule first adsorbs onto the catalyst surface, leading to two consecutive protonation steps and the formation of N_2H and N_2H_2 intermediates at potentials below −0.4 V. N_2H_2 is identified as the predominant intermediate in ammonia production. For the first time, this study, utilizing isotope labeling and OLEMS, has enabled the identification of key NRR intermediates, the correlation of NH_3 production with N_2 consumption as a function of applied potential, and has provided crucial insights into this important reaction. A comprehensive understanding of the NRR mechanism will facilitate the development of high-performance catalysts.

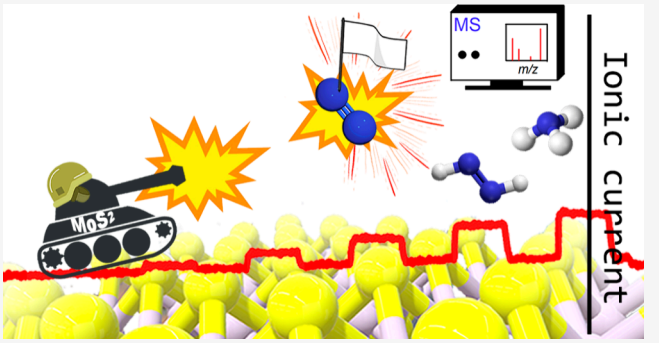

KEYWORDS: *nitrogen reduction reaction (NRR), MoS_2 electrocatalysts, OLEMS (online electrochemical mass spectrometry), reaction mechanism, isotope labeling*

INTRODUCTION

Electrochemical nitrogen reduction to ammonia, conducted under ambient temperature and pressure, has emerged as a promising alternative to the conventional Haber-Bosch process,[1−3] primarily because of its potential to reduce CO_2 emissions. This sustainable energy conversion process, utilizing N_2 and H_2O, not only reduces the polluting gas emissions but also decreases dependence on petroleum products, thereby contributing to a more sustainable energy matrix.[4,5] However, the nitrogen reduction reaction (NRR) faces significant challenges due to the high stability of the N_2 molecule and the scarcity of active and efficient catalysts.

One of the main barriers to overcoming the NRR (eq 1)[6] are (i) the high energy barrier (941 kJ mol^{-1}) required to break the strong triple bond of the nitrogen molecule, (ii) the low solubility of N_2 in aqueous systems (approximately 0.66 mmol L^{-1}),[7] (iii) slow reaction kinetics[7,8] and (iv) the competing hydrogen evolution reaction (HER) (eq 2).[6]

$$N_2 + 6H^+ + 6e^- \leftrightharpoons 2NH_{3(g)} \quad (1)$$

$$2H^+ + 2e^- \leftrightharpoons H_{2(g)} \quad (2)$$

Density functional theory (DFT) studies have been widely employed to investigate NRR reaction mechanisms, determine activation energies, and predict promising materials for these reactions using Sabatier plots.[9] The most commonly proposed mechanism in DFT studies to describe the NRR on metal surfaces at low temperatures and pressures is the associative mechanism. In this mechanism, the nitrogen molecule adsorbs onto the catalytic surface (*N_2 end-on), and its triple bond is broken through a series of reduction steps via two distinct pathways: the alternating pathway (eqs 3−8) and the distal pathway (eqs 9−15) (Table 1).

In the alternating pathway, the N_2 molecule first adsorbs onto the surface, followed by three hydrogenation steps that lead to the formation of the ammonia molecule (eq 7). Then,

Received: October 18, 2024
Revised: December 27, 2024
Accepted: January 9, 2025
Published: January 17, 2025

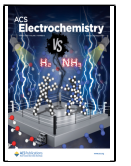

Table 1. DFT Associative Mechanism for NRR[a]

Alternate pathway	Distal pathway
$N_2 + * \rightarrow {}^*N_2$ (3)	$N_2 + * \rightarrow {}^*N_2$ (9)
${}^*N_2 + e^- + H^+ \rightarrow {}^*NNH$ (4)	${}^*N_2 + e^- + H^+ \rightarrow {}^*NNH$ (10)
${}^*NNH + e^- + H^+ \rightarrow {}^*NHNH$ (5)	${}^*NNH + e^- + H^+ \rightarrow {}^*NHNH_2$ (11)
${}^*NHNH + e^- + H^+ \rightarrow {}^*NHNH_2$ (6)	${}^*NNH_2 + e^- + H^+ \rightarrow {}^*N + NH_3$ (12)
${}^*NHNH_2 + e^- + H^+ \rightarrow {}^*NH_2 + NH_3$ (7)	${}^*N + e^- + H^+ \rightarrow {}^*NH$ (13)
$NH_2 + e^- + H^+ \rightarrow NH_3 + *$ (8)	${}^*NH + e^- + H^+ \rightarrow {}^*NH_2$ (14)
	${}^*NH_2 + e^- + H^+ \rightarrow NH_3 + *$ (15)

[a]* indicates active site.

Table 2. NRR Studies Based on Techniques Such As FTIR and DEMS Presented in the Literature

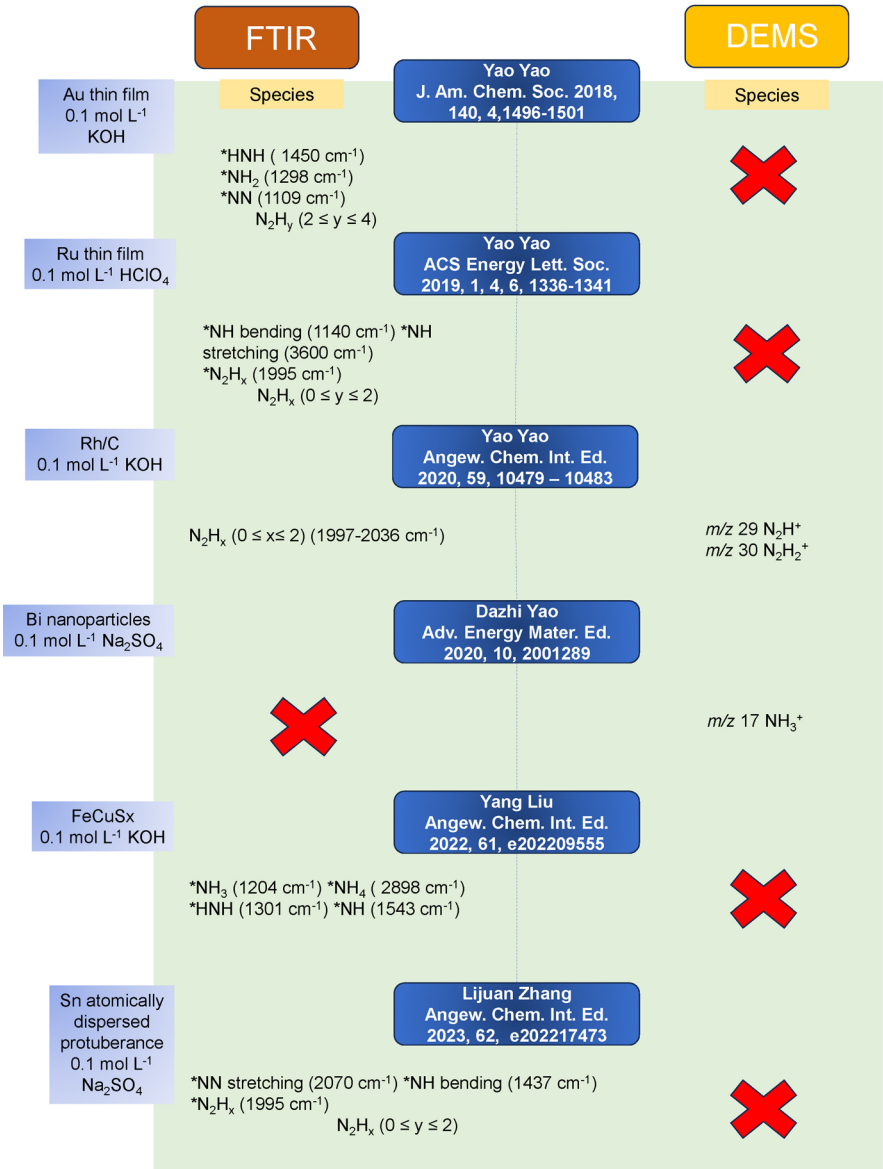

the $^*NH_2$ intermediate then combines with H^+ to form another molecule of NH_3 (eq 8). In the distal pathway, hydrogenation occurs on only one nitrogen atom until NH_3 is formed (eq 12), leaving the *N species adsorbed on the surface. This adsorbed *N species undergoes two more hydrogenations, forming $^*NH_2$ (eqs 13 and 14) and ultimately producing NH_3 (eq 15).[10−13]

However, most experimental studies on NRR using various types of electrocatalysts focus primarily on quantifying ammonia, often lacking detailed mechanistic investigations.

https://doi.org/10.1021/acselectrochem.4c00135
ACS Electrochem. 2025, 1, 294−302

Ammonia quantification has typically been performed using UV−vis spectroscopy, ^{1}H NMR,[14−16] and chromatography.[17−19] Some studies have highlighted the issue of false positives in ammonia detection, which can arise from contamination of the electrolyte, catalyst, or reagent gases with NO_x species.[20,21] Recently, Suryanto et al. (2019)[22] addressed the challenges of proving that ammonia produced during NRR originates exclusively from the electrochemical reduction of N_2. This work emphasized the importance of reagent gas purity and the need for rigorous measurement protocols.

Mechanistic studies on NRR using Fourier transform infrared spectroscopy (FTIR) and differential electrochemical mass spectrometry (DEMS) are less common. A summary of these studies, presented in chronological order, is provided in Table 2, followed by a brief discussion of the relevant literature.

Yao et al.,[23] in their study of NRR during cathodic scans (0.3 to −0.1 V vs. RHE) on Au surfaces in 0.1 mol L^{-1} KOH, used surface-enhanced infrared absorption spectroscopy (SEIRAS) techniques to detect N_2H_y species at potentials below 0.0 V. These species included H−N−H bending (1453 cm^{-1} band), -NH_2 wagging (1453 cm^{-1} band), and N−N stretching (1109 cm^{-1} band), suggesting that NRR on Au surfaces follows an associative mechanism.

Another study[24] employing the SEIRAS technique investigated a thin film of Ru in 0.1 mol L^{-1} $HClO_4$ and identified the following adsorbed species: *NH bending (band at 1140 cm^{-1}), *NH stretching (band at 3600 cm^{-1}), and *N_2H_x (band at 1995 cm^{-1}, where $0 \leq x \leq 2$). On the Ru surface, species such as *N_2H_x can desorb as N_2H_2, an unstable intermediate that decomposes into NH_3 and N_2 in the electrolyte. This suggests that the decomposition pathway described by eq 16 is the predominant reaction. Similar experiments in KOH did not detect bands associated with the adsorption of nitrogen species.

$$3N_2H_2 \rightleftharpoons 2NH_3 + 2N_2 \quad (16)$$

In 2020, Yao et al.[25] investigated the NRR using SEIRAS and DEMS techniques on the surface of Rh in 0.1 mol L^{-1} KOH. SEIRAS detected N_2H_x species ($0 \leq x \leq 2$) through bands at 1997−2036 cm^{-1}, with the N═N stretching mode around 2020 cm^{-1}, within a potential range of 0.2 to −0.4 V vs. RHE. DEMS monitoring identified the following species: m/z 2 (H_2^+), m/z 29 (N_2H^+), m/z 30 ($N_2H_2^+$), and m/z 31 ($N_2H_3^+$). The authors noted that the m/z 29 signal was a pulse resulting from H_2 bubbles at potentials below −0.3 V vs. RHE. The m/z 30 and 31 signals were not observed, suggesting that N_2H_2 decomposes easily in the electrolyte. The study proposed that the electrochemical process involves the transfer of two electrons to form N_2H_2, which then decomposes in the electrolyte to yield NH_3 and N_2 (eq 16).

In another NRR study, Yao et al.[8] used Bi nanoparticles in 0.1 mol L^{-1} Na_2SO_4 and quantified NH_3 production via UV-Vis, ion chromatography, and ^{1}H NMR, while monitoring volatile species using DEMS. The authors polarized the system at −0.7 V vs. RHE for 5 min and observed the m/z 17 signal, which was attributed to NH_3^+, and m/z 30 ($N_2H_2^+$) in the extended DEMS range. They proposed that NRR could occur via either the decomposition pathway (eq 16) or an associative pathway.

Liu et al.,[26] using $FeCuS_x$ catalysts in 0.1 mol L^{-1} KOH, quantified NH_3 with UV-Vis and ^{1}H NMR spectra. Mechanistic studies using FTIR and DFT revealed the following species at a potential of −0.1 V vs. RHE (0 to 150 s): *NH_3 (band at 1204 cm^{-1}), *NH_4 (band at 2898 cm^{-1}), −N−N stretching (band at 1131 cm^{-1}), N_2H_y or −H−N−H bending (bands at 1301/1543 cm^{-1}), and −N−H stretching (band at 3010 cm^{-1}). The authors suggested that the reaction on the $FeCuS_x$ surface follows an associative alternating pathway mechanism.

Using Sn ADP catalysts in 0.1 mol L^{-1} Na_2SO_4, Lijuan Zhang et al.[27] quantified NH_3 via UV-Vis and ^{1}H NMR. They employed ATR-SEIRAS to monitor possible reaction intermediates over a potential range of 0.4 to −0.4 V vs. RHE. The intensity of bands increased with cathodic potential, peaking at −0.3 V, which was identified as optimal for the catalyst. Two species were detected starting at −0.1 V: N═N stretching (band at 2070 cm^{-1}) and N−H bending vibrations (band at 1437 cm^{-1}). The increase in these species with reaction time suggested the accumulation of intermediate N_2H_x on the Sn ADP electrocatalyst. Combined with DFT results, this study indicates that the distal pathway is the most likely.

In summary, a review of FTIR and DEMS results shows inconsistencies in the proposed reaction mechanisms for NRR. Despite DEMS confirming some intermediates identified by FTIR, the resolution of the analyzed species remains low. Further fundamental studies are necessary to clarify the reaction stages and develop more efficient electrocatalysts for NH_3 production.

In our previous study on ammonia oxidation, we significantly increased the detection of reaction products using an experimental setup combining OLEMS and a gas diffusion electrode.[28] We adapted this methodology to study NRR, using both labeled and unlabeled compounds to identify key intermediates as a function of applied potential. The MoS_2 catalysts exhibits metastable phases with a high density of localized electrons, which promote N_2 adsorption and the formation of strong interactions with the metal (Mo−N). These interactions lower the barriers for N≡N bond cleavage, making MoS_2 an attractive material for NRR.[29,30] Thus, we present potentiostatic and potentiodynamic studies in alkaline media on MoS_2 electrodes, utilizing OLEMS and UV-Vis spectroscopy for identifying gaseous and solution products.

EXPERIMENTAL SECTION

The working electrode used was a gas diffusion electrode (GDE) composed of carbon cloth, with a geometric area of 1.9 cm^2, prepared by depositing the commercial catalyst onto the GDE. The reference electrode was Hg|HgO (1.0 mol L^{-1} NaOH), and the counter electrode was graphite. The compartments of the electrochemical cell were separated by a Nafion 115 membrane (Figure S1).

To prepare the working electrode, 4.7 mg of MoS_2 was used, along with approximately 0.3 mg of Vulcan® Carbon to optimize the catalyst's conductivity, followed by adding 37 μL of a 5% w/v Nafion® solution. The mixture was subjected to ultrasonic treatment for 30 min and then transferred to the carbon cloth GDE. The electrode was dried at 80 °C for 1 h.

The chronoamperometric (CA) experiments were carried out using potential steps of −0.3, −0.4, −0.5, −0.6, −0.7, −0.8, −0.9, and −1.0 V vs. RHE, with each step maintained for 600 seconds. Measurements were conducted at −0.1 V for 600 seconds between consecutive potential steps. For cyclic voltammetry (CV), scans were performed over a potential range from 0.0 to −1.0 V vs. RHE, with a scan rate of 1 mV s^{-1}

https://doi.org/10.1021/acselectrochem.4c00135
ACS Electrochem. 2025, 1, 294−302

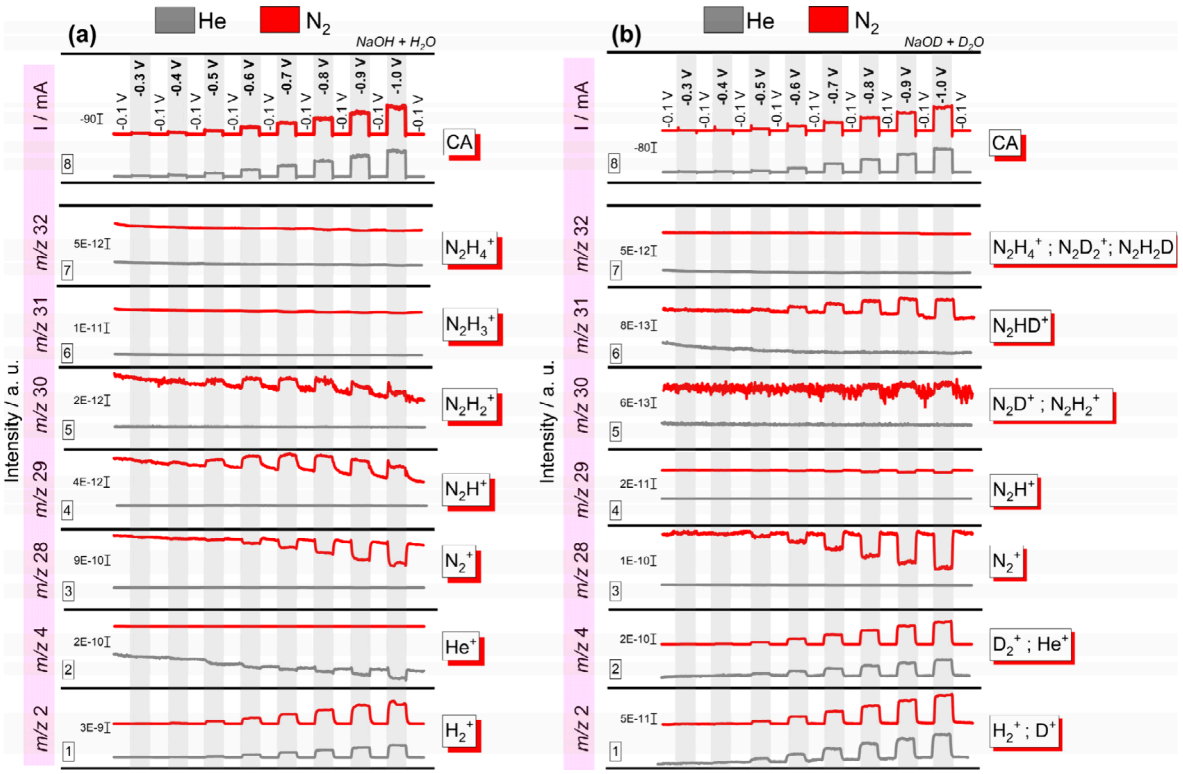

Figure 1. OLEMS mass signal results for MoS_2. (a) CA-MS in 1.0 mol L^{-1} NaOH electrolyte. (b) CA-MS in 1.0 mol L^{-1} NaOD + D_2O electrolyte. In both cases, the gray and red lines correspond to He and N_2, respectively. N_2 in the cathodic chamber.

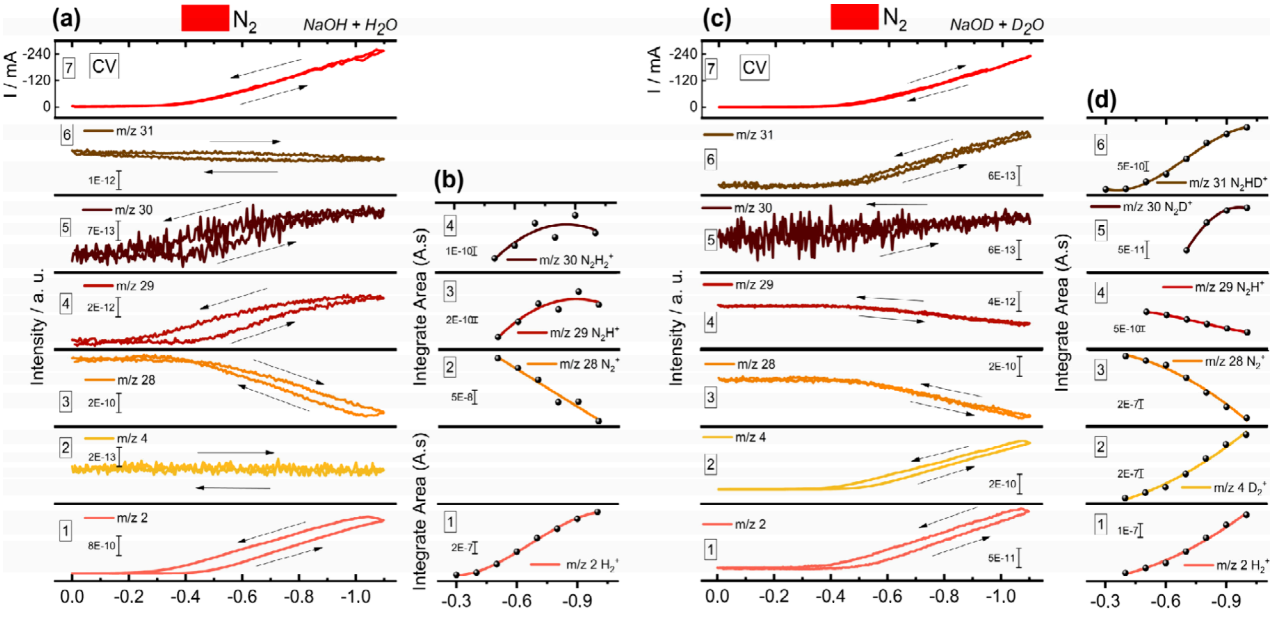

Figure 2. OLEMS mass signal results for MoS_2. (a) CV-MS at a scan rate of 1 mV s^{-1} in 1.0 mol L^{-1} NaOH electrolyte in the presence of N_2. (b) Integral of ionic charge as a function of the applied potential obtained from CA-MS in 1.0 mol L^{-1} NaOH electrolyte in the presence of N_2. (c) CV-MS at a scan rate of 1 mV s^{-1} in NaOD + D_2O electrolyte in the presence of N_2. (d) Integral of ionic charge as a function of the applied potential obtained from CA-MS in NaOD + D_2O electrolyte. N_2 in the cathodic chamber.

. A detailed summary of the experimental conditions is provided in Table S1.

The distribution of products from the nitrogen reduction reaction was monitored using online electrochemical mass spectrometry (OLEMS), which analyzes the generated gaseous products. The mass spectrometer used was the OmniStar® GSD 301 from Pfeiffer Vacuum, model Prisma QMS 200, with the following parameters: ionization energy of 70 eV, emission current of 1 mA, and a pressure in the order of 10^{-6} mbar. The methodology for studying the NRR on MoS_2 catalysts in 1.0 mol L^{-1} NaOH, using a Nafion 115 membrane for separation of the anodic and cathodic compartments, is illustrated in Figure S1.

https://doi.org/10.1021/acselectrochem.4c00135
ACS Electrochem. 2025, 1, 294−302

Quantification of NH_3 was performed using the Berthelot method, where alkaline phenol and hypochlorite react with ammonia to form indophenol blue, which is proportional to the concentration of ammonium in solution. Hydrazine was quantified using the Watt and Chrisp method. The details of the experiments are summarized in Supporting Information.

RESULTS AND DISCUSSION

Physical characterizations of the material are presented in Figures S2 to S5. The experimental protocol is detailed in the supplementary information to minimize contamination from gas, electrolyte, catalyst, or the separation membrane. The gases used were N_2 6.0 (99.9999% purity) and He 4.5 FID.

Figures 1a1−1a8 display chronoamperometry (CA) results and CA-MS signals for various volatile species as a function of the applied potential: m/z 32 ($N_2H_4^+$), 31 ($N_2H_3^+$), 30 ($N_2H_2^+$), 29 (N_2H^+), 28 (N_2^+), 4 (He^+), and 2 (H_2^+). Results for the NRR are shown in red, while measurements in the absence of nitrogen (i.e., in helium) are depicted in gray.

Figures 2a1−2a7 present cyclic voltammetry (CV) and CV-MS signals for the same volatile species in the presence of N_2 in 1.0 mol L^{-1} NaOH. Figures 2b1−2b4 show the integrals of the ionic charges of the species representing production or consumption as a function of the applied potential, derived from Figures 1a1−1a7. Results obtained in the absence of nitrogen are shown in Figures S6a1−S6a7. The following is a detailed analysis of each monitored species.

The CA-MS results for the m/z 2 signal, attributed to hydrogen (Figure 1a1), in the absence of nitrogen (gray line), indicate that only the hydrogen evolution reaction (HER) occurs. As the cathode potential increases, there is a corresponding increase in hydrogen production, demonstrating that the MoS_2 catalyst is active for HER.[31−34] Additionally, the m/z 4 signal (Figure 1a2), attributed to helium, showed variations only due to the pressure changes from hydrogen production. In the presence of nitrogen, as shown by the red line in Figure 1a1, hydrogen formation behaves similarly to that observed in a helium atmosphere. These findings are corroborated by CV-MS data, which show increased hydrogen production with applied cathode potential (Figure 2a1). Figure 2b1 displays the integral of the ionic charge for the m/z 2 signal, showing consistent behavior with the CV-MS results.

The m/z 28 signal, assigned to N_2, demonstrates a consumption band in the CA-MS data starting at −0.4 V and increasing with further cathode potential (Figure 1a3, red line). This band was not observed in the presence of He (Figure 1a3, gray line). CV-MS results in Figures 2a3 and S6a3 confirm that N_2 consumption occurs alongside HER when N_2 is present. Moreover, the CV-MS studies reveal a slight hysteresis between forward and reverse scans and increased N_2 consumption, suggesting that the surface was not blocked by *N, as some DFT studies propose.[10−13] Figure 2b2 shows the integral of the ionic charge for the m/z 28 signal, indicating similar consumption behavior as observed in the CV-MS results. It is noteworthy that no mass spectroscopy studies on the NRR have reported nitrogen consumption.

The signals corresponding to m/z 29 and m/z 30 were assigned to the species N_2H^+ and $N_2H_2^+$, respectively, and are shown in Figures 1a4 and 1a5. The figures display the CA-MS results both in the absence (gray lines) and presence of N_2 (red lines). During the NRR, the production of these species was clearly monitored with the applied potential, indicating their involvement in NH_3 production. These species are not detected in the absence of N_2 (gray lines). The m/z 29 signal could partially arise from the fragmentation of the m/z 30 species. However, prior studies involving FTIR data[24,25,27] have reported the production band for N_2H_x ($1 \leq x \leq 2$) species under applied potential. Furthermore, Yao et al.[8] detected N_2H^+ (m/z 29) using DEMS with a low-resolution signal at high cathode potentials (> −0.7 V vs. RHE), noting that this species appeared only when H_2 bubbles formed and did not detect m/z 30 or 31. In contrast, our results detected both N_2H^+ (m/z 29) and $N_2H_2^+$ (m/z 30) using OLEMS over a wide range of potentials through CA and CV experiments. These species appeared concurrently with H_2 (m/z 2), starting at −0.4 V vs. RHE. CV-MS results (Figures 2a4 and 2a5) confirm the production of N_2H and N_2H_2 from −0.4 V vs. RHE. In the absence of N_2, m/z 29 and m/z 30 signals were not detected (Figure S6a4 and S6a5). Slight hysteresis in direct and reverse scans for both species indicates increased production during the reverse scan, corroborating the rise in N_2 consumption (Figure 2a3). Figures 2b3 and 2b4 display the ionic charge integrals for m/z 29 and 30, respectively, showing behavior consistent with the CV-MS results. The detection of N_2H and N_2H_2 species as a function of potential is a key finding in our NRR studies.

DFT studies suggested that $N_2H_3^+$ could be involved in the ammonia formation mechanism (Table 1, eq 7). However, we did not detect the m/z 31 signal, attributed to $N_2H_3^+$,[35] in either CA-MS or CV-MS results (Figures 1a6 and 2a6). This signal was also absent in the presence of helium (Figure 1a6 and S6a6). Additionally, theoretical studies have proposed that hydrazine might act as a reaction intermediate.[6,36−38] Figure 1a7 presents results for the m/z 32 signal, attributed to $N_2H_4^+$,[35] but no formation of this species was observed for the NRR (red line) or in the presence of He (gray line). UV-Vis analysis using the Watt method and Chrisp[39] did not identify hydrazine formation (Figure S13), confirming that this species did not form on the MoS_2 surface during NRR.

Yao et al.[8] monitored the m/z 17 signal, attributed to NH_3^+, in aqueous solution and associated it with ammonia production. However, their results showed m/z 17 in both the presence and absence of N_2, without presenting the m/z 18 signal to account for water contributions. In aqueous solutions, hydrogen production can carry water vapor to the mass detector, as confirmed by our results with signals for m/z 17 (OH^+) and m/z 18 (H_2O^+) (Figure S7a1 and S7a2). The influence of water on these m/z signals was also confirmed in helium atmosphere experiments (Figure S7b1 and S7b2).

Thus far, we have analyzed the OLEMS results for NRR in NaOH and H_2O. To validate these findings, we conducted additional measurements using isotope labeling with NaOD and D_2O solutions. The signal m/z for each hydrogen-containing species changed due to the presence of deuterium, as detailed in Table S3. The CA-MS results for volatile species monitored as a function of the applied potential are shown in Figures 1b1 to 1b7. These figures correspond to the following mass signals: m/z 32 ($N_2H_4^+$ or $N_2D_2^+$), 31 (N_2HD^+), 30 ($N_2H_2^+$ or N_2D^+), 29 (N_2H^+), 28 (N_2^+), 4 (D_2^+ or He^+), and 2 (H_2^+ or D^+), with CA results presented in Figure 1b8. In red, the results for NRR are shown, and in gray, measurements in the absence of nitrogen (i.e., helium atmosphere) in NaOD/D_2O 1.0 mol L^{-1} are depicted.

In deuterated compounds under the monitored reduction potentials, the mass signals m/z 2 and m/z 4 confirmed the presence of H_2^+/D^+ and D_2^+ species in N_2 and He. The CV-

https://doi.org/10.1021/acselectrochem.4c00135
ACS Electrochem. 2025, 1, 294−302

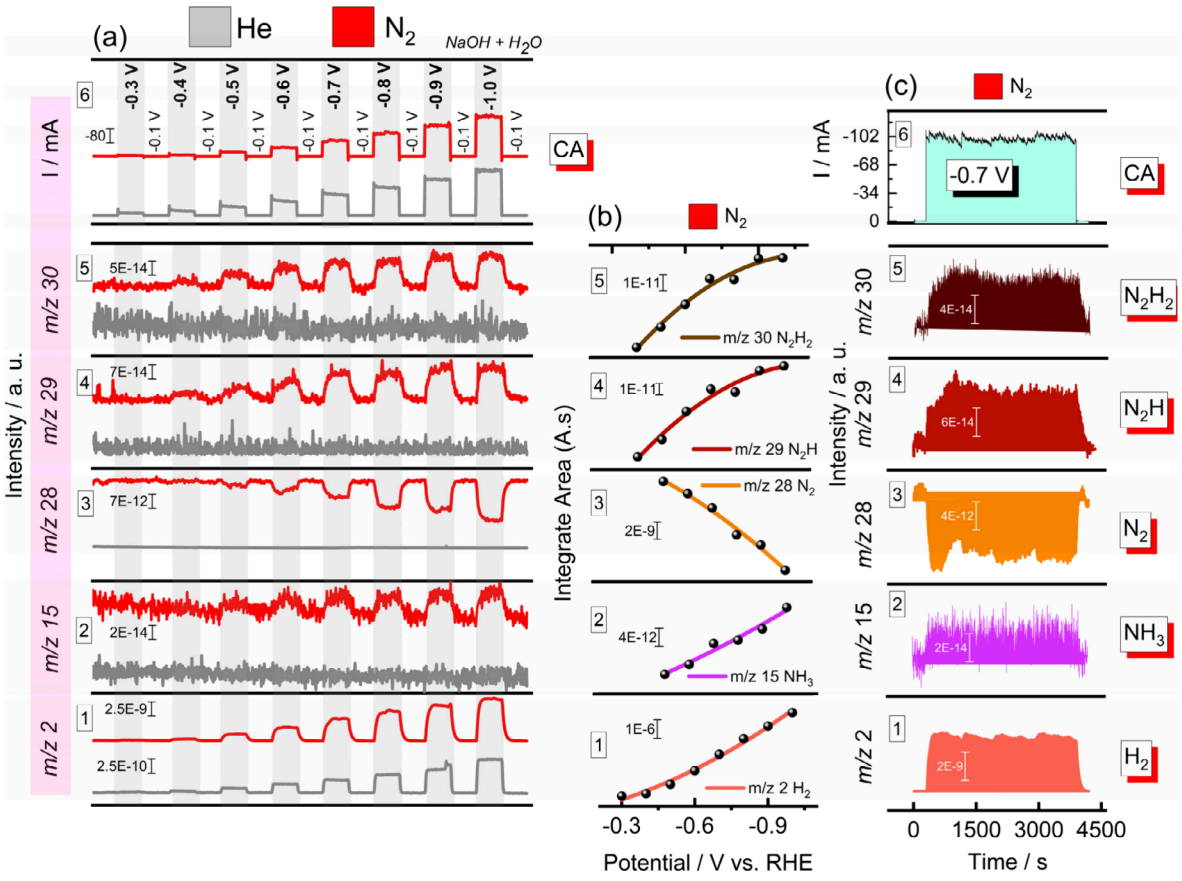

Figure 3. OLEMS mass signal results for MoS_2. (a) CA-MS in 1.0 mol L^{-1} NaOH electrolyte (gray and red lines correspond to He and N_2, respectively). (b) Integral of ionic charge as a function of the applied potential obtained from CA-MS in 1.0 mol L^{-1} NaOH electrolyte in the presence of N_2. (c) CA-MS measurements of MoS_2 polarized at −0.7 V vs. RHE for 1 h. He in the cathodic chamber.

MS results with isotope labeling (Figures 2c1 to 2c7) display mass signals for volatile species as a function of the applied potential: *m/z* 2, 4, 28, 29, 30, and 31, with corresponding CV results presented from bottom to top in N_2. For He, similar results are shown in Figures S6b1−S6b7, where only H_2 and D_2 were observed. Figures 2d1−2d6 show the integrals of ionic charges as a function of the applied potential for species that exhibited production or consumption, confirming the CV-MS results observed without labeling compounds.

In summary, the isotope labeling experiments confirmed the shift in mass signals due to the presence of deuterium. The presence of N_2H^+ (*m/z* 29) was confirmed by a shift to *m/z* 30 for N_2D^+ species (Figure 1b5, red line). The $N_2H_2^+$ (*m/z* 30) was confirmed by a shift to *m/z* 31 for N_2HD^+, and the absence of $N_2D_2^+$ species can be attributed to the isotopic distribution.[40] N_2 consumption during polarization with deuterium (Figure 1b3, red line) showed similar behavior to the system without deuterium (Figure 1a3, red line). The contributions of water to the NH_3 production signal could not be separated (Table S3), as shown in Figure S8a1 to S8a4, with similar findings in the helium atmosphere (Figure S8b1 to S8b4). No signals for $N_2H_2D^+$, $N_2H_3D^+$, $N_2H_2D_2^+$, and $N_2D_4^+$ were observed (Figures 1b7, S10a2, S10a3, and S10a4), confirming the absence of $N_2H_3^+$ and $N_2H_4^+$ species in the NRR. The results for these masses in He, shown in Figures S10b1−S10b4, were consistent with these findings.

To verify NH_3 production, we also monitored the *m/z* 15 signal,[8] although this signal is influenced by fragmentation of the nitrogen signal (*m/z* 14, Figure S11). To exclude this interference, we conducted experiments with He gas placed behind the cathode chamber during NRR. Results for *m/z* 2, 15, 28, 29, and 30 are presented in Figures 3a1−3a5, with red lines indicating N_2 (in solution) and gray lines indicating helium. CA results are shown in Figure 3a6. The CA-MS results indicate NH_3 production starting from −0.5 V vs. RHE, immediately after the formation of intermediates N_2H and N_2H_2 and the onset of N_2 consumption. MS results for N_2H and N_2H_2 species showed similar trends to those with N_2 in the chamber but with lower signal intensity (Figures 1a4−1a5 and 3a4−3a5). The results for He (Figure 3a, gray line) showed only HER, as expected. Figures 3b1−3b5 display the integrals of ionic charges from Figures 3a1−3a5 (red lines), confirming N_2 consumption and production of H_2, NH_3, N_2H, and N_2H_2. NH_3 production in aqueous medium was further confirmed using UV-Vis analysis with the Berthelot method[41−43] (Figure S12).

Furthermore, to study the behavior of species consumption/production over time, we performed a CA-MS experiment at −0.7 V vs. RHE for 1 h, with results shown in Figures 3c1 to 3c6 for *m/z* 2, 15, 28, 29, and 30, and CA results. These results confirmed that N_2 consumption and production of NH_3, N_2H, and N_2H_2 remained constant with the applied potential, suggesting no formation of adsorbed species blocking active sites, in line with CV-MS results (Figures 2a3, 2a4, 2a5) which showed slight hysteresis with increased production in the reverse scan.

A review of the literature, combined with theoretical (DFT) and experimental data, shows that there is no consensus on the

https://doi.org/10.1021/acselectrochem.4c00135
ACS Electrochem. 2025, 1, 294−302

Scheme 1. Pathways for Electrochemical Reduction of Nitrogen on the MoS_2 Surface

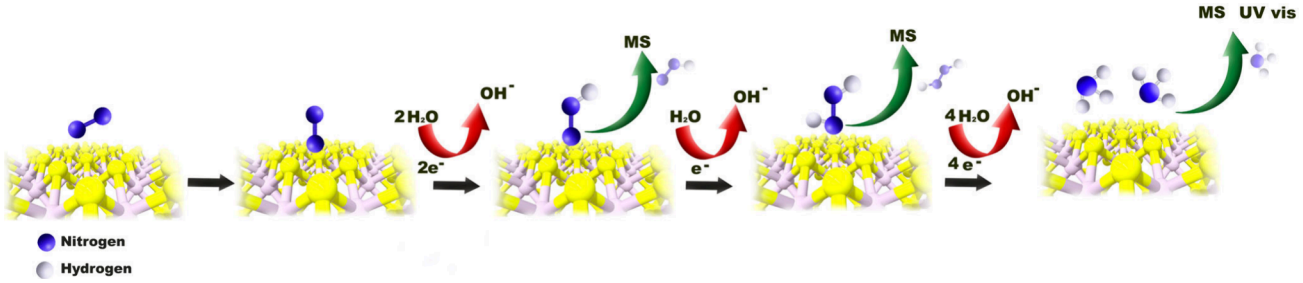

species involved in the NRR mechanism. However, most studies suggest that N_2H_y ($1 \leq y \leq 2$) species are intermediates in the ammonia formation mechanism. In this study, using OLEMS (CA-MS and CV-MS) and UV-Vis, we present several novel findings: (i) Detection of N_2H^+ and $N_2H_2^+$ as intermediates from −0.4 V vs. RHE, confirmed by isotope labeling; (ii) Detection of N_2 consumption from −0.4 V vs. RHE; (iii) Production of NH_3 (m/z 15) starting at −0.5 V, following detection of intermediates N_2H and N_2H_2 and N_2 consumption, also confirmed by UV-Vis; (iv) Absence of $N_2H_3^+$ and $N_2H_4^+$, confirmed by isotope labeling, with N_2H_4 also not detected by UV-Vis, allowing us to exclude mechanisms involving these species; (v) CV-MS results showing slight hysteresis with increased production in the reverse scan, corroborated by prolonged CA-MS, indicating no formation of adsorbed species blocking active sites. Based on these results, we propose a possible NRR mechanism on MoS_2 surfaces, as illustrated in Scheme 1. In this mechanism, the N_2 molecule adsorbs on the catalyst, followed by two consecutive protonation to form N_2H and N_2H_2 species at potentials below −0.4 V, with N_2H_2 being the main intermediate for ammonia production.

CONCLUSION

Understanding the mechanisms and reaction pathways of the NRR is crucial for advancing this field. Despite the competition between the NRR and HER, our study focused on the NRR in alkaline media using MoS_2 electrodes and OLEMS and UV-vis spectroscopy, with both labeled and unlabeled compounds. By employing pure gases, precise electrolytes, and a rigorous measurement protocol, we achieved a high-resolution detection of key reaction intermediates.

Our findings reveal the formation of the intermediates N_2H and N_2H_2, along with the consumption of N_2 and subsequent production of NH_3 as a function of applied potential. This detection was confirmed with unprecedented resolution using OLEMS. Notably, we did not detect the species N_2H_3 and N_2H_4, which have been proposed in some literature mechanisms, using either OLEMS or UV-vis techniques.

The carefully developed measurement protocol in this study has allowed us to identify the critical intermediates involved in ammonia production and propose a pathway for the NRR. This approach not only enhances our understanding of reaction mechanisms on different surfaces but also paves the way for developing improved catalysts that enhance nitrogen electroreduction while minimizing hydrogen evolution.

ASSOCIATED CONTENT

Supporting Information

The Supporting Information is available free of charge at https://pubs.acs.org/doi/10.1021/acselectrochem.4c00135.

OLEMS cell, OLEMS mass signal standard, physical characterization (TGA, DRX, XPS and TEM), OLEMS results for CV-MS and CA-MS window opening experiment, the protocol of electrochemical experiments and quantification of products (PDF)

AUTHOR INFORMATION

Corresponding Author

Joelma Perez − *São Carlos Institute of Chemistry, University of São Paulo (USP), 13560-970 São Carlos, Brazil;* orcid.org/0000-0003-3307-4711; Email: jperez@iqsc.usp.br

Author

Rodrigo Gomes de Araujo − *São Carlos Institute of Chemistry, University of São Paulo (USP), 13560-970 São Carlos, Brazil*

Complete contact information is available at: https://pubs.acs.org/10.1021/acselectrochem.4c00135

Author Contributions

The manuscript was written through contributions of all authors. All authors have given approval to the final version of the manuscript.

Funding

This work was supported by São Paulo Research Foundation (FAPESP) (grant no. 2019/22183-6). The Article Processing Charge for the publication of this research was funded by the Coordination for the Improvement of Higher Education Personnel - CAPES (ROR identifier: 00x0ma614).

Notes

The authors declare no competing financial interest.

ACKNOWLEDGMENTS

This study was financed in part by the Coordenação de Aperfeiçoamento de Pessoal de Nível Superior − Brasil (CAPES) − Finance Code 001. The authors thank the FAPESP, J.P. thank CNPq (142482/2019-6) and R.G.A. thank Capes (88887.928038/2023-00) for the fellowships granted.

REFERENCES

(1) Du, H.; Yang, C.; Pu, W.; Zeng, L.; Gong, J. Enhanced Electrochemical Reduction of N_2 to Ammonia over Pyrite FeS_2 with Excellent Selectivity. *ACS Sustain. Chem. Eng.* **2020**, *8*, 10572−10580.

(2) Su, H.; Chen, L.; Chen, Y.; Si, R.; Wu, Y.; Wu, X.; Geng, Z.; Zhang, W.; Zeng, J. Single Atoms of Iron on MoS_2 Nanosheets for N_2

Electroreduction into Ammonia. *Angew. Chem. Int. Ed.* **2020**, *59*, 20411−20416.
(3) Ma, H.; Chen, Z.; Wang, Z. Electroreduction of Nitrogen to Ammonia on Nanoporous Gold. *Nanoscale* **2021**, *13*, 1717−1722.
(4) Chen, J. G.; Crooks, R. M.; Seefeldt, L. C.; Bren, K. L.; Bullock, R. M.; Darensbourg, M. Y.; Holland, P. L.; Hoffman, B.; Janik, M. J.; Jones, A. K.; et al. Beyond Fossil Fuel-Driven Nitrogen Transformations. *Science* **2018**, *360*, No. eaar6611.
(5) Foster, S. L.; Bakovic, S. I. P.; Duda, R. D.; Maheshwari, S.; Milton, R. D.; Minteer, S. D.; Janik, M. J.; Renner, J. N.; Greenlee, L. F. Catalysts for Nitrogen Reduction to Ammonia. *Nat. Catal.* **2018**, *1*, 490−500.
(6) van der Ham, C.; Koper, M.; Hetterscheid, D. Challenges in Reduction of Dinitrogen by Proton and Electron Transfer. *Chem. Soc. Rev.* **2014**, *43*, 5183−5191.
(7) Tang, C.; Qiao, S. How to Explore Ambient Electrocatalytic Nitrogen Reduction Reliably and Insightfully. *Chem. Soc. Rev.* **2019**, *48*, 3166−3180.
(8) Yao, D.; Tang, C.; Li, L.; Xia, B.; Vasileff, A.; Jin, H.; Zhang, Y.; Qiao, S.-Z. In Situ Fragmented Bismuth Nanoparticles for Electrocatalytic Nitrogen Reduction. *Adv. Energy Mater.* **2020**, *10* DOI: 10.1002/aenm.202001289.
(9) Cui, X.; Tang, C.; Zhang, Q. A Review of Electrocatalytic Reduction of Dinitrogen to Ammonia under Ambient Conditions. *Adv. Energy Mater.* **2018**, *8*, No. 1800369.
(10) Shetty, A. U.; Sankannavar, R. Exploring Nitrogen Reduction Reaction Mechanisms in Electrocatalytic Ammonia Synthesis: A Comprehensive Review. *J. Energy Chem.* **2024**, *92*, 681−697.
(11) Skúlason, E.; Bligaard, T.; Gudmundsdóttir, S.; Studt, F.; Rossmeisl, J.; Abild-Pedersen, F.; Vegge, T.; Jónsson, H.; Nørskov, J. K. A Theoretical Evaluation of Possible Transition Metal Electro-Catalysts for N_2 Reduction. *Phys. Chem. Chem. Phys.* **2012**, *14*, 1235−1245.
(12) Azofra, L. M.; Li, N.; MacFarlane, D. R.; Sun, C. Promising Prospects for 2D d^2−d^4 M_3C_2 Transition Metal Carbides (MXenes) in N_2 Capture and Conversion into Ammonia. *Energy Environ. Sci.* **2016**, *9*, 2545−2549.
(13) Singh, A. R.; Rohr, B. A.; Statt, M. J.; Schwalbe, J. A.; Cargnello, M.; Nørskov, J. K. Strategies Toward Selective Electrochemical Ammonia Synthesis. *ACS Catal.* **2019**, *9*, 8316−8324.
(14) Biswas, A.; Ghosh, B.; Dey, R. S. Refining the Spectroscopic Detection Technique: A Pivot in the Electrochemical Ammonia Synthesis. *Langmuir* **2023**, *39*, 3810−3820.
(15) Giner-Sanz, J. J.; Leverick, G.; Pérez-Herranz, V.; Shao-Horn, Y. Optimization of the Salicylate Method for Ammonia Quantification from Nitrogen Electroreduction. *J. Electroanal. Chem.* **2021**, *896*, No. 115250.
(16) Assafiri, A.; Jia, C.; Thomas, D. S.; Hibbert, D. B.; Zhao, C. Fast and Sensitive Detection of Ammonia from Electrochemical Nitrogen Reduction Reactions by ^{1}H NMR with Radiation Damping. *Small Methods* **2024**, *8*, No. 2301373.
(17) Kolen, M.; Ripepi, D.; Smith, W.; Burdyny, T.; Mulder, F. Overcoming Nitrogen Reduction to Ammonia Detection Challenges: The Case for Leapfrogging to Gas Diffusion Electrode Platforms. *ACS Catal.* **2022**, *12*, 5726−5735.
(18) Ripepi, D.; Zaffaroni, R.; Kolen, M.; Middelkoop, J.; Mulder, F. M. Operando Isotope Selective Ammonia Quantification in Nitrogen Reduction Studies via Gas Chromatography-Mass Spectrometry. *Sustain. Energy Fuels* **2022**, *6*, 1945−1949.
(19) Duan, G. Y.; Ren, Y.; Tang, Y.; Sun, Y. Z.; Chen, Y. M.; Wan, P. Y.; Yang, X. J. Improving the Reliability and Accuracy of Ammonia Quantification in Electro- and Photochemical Synthesis. *ChemSusChem* **2020**, *13*, 88−96.
(20) Choi, J.; Suryanto, B. H. R.; Wang, D.; Du, H.-L.; Hodgetts, R. Y.; Ferrero Vallana, F. M.; MacFarlane, D. R.; Simonov, A. N. Identification and Elimination of False Positives in Electrochemical Nitrogen Reduction Studies. *Nat. Commun.* **2020**, *11*, 5546.
(21) Dabundo, R.; Lehmann, M. F.; Treibergs, L.; Tobias, C. R.; Altabet, M. A.; Moisander, P. H.; Granger, J. The Contamination of Commercial $^{15}N_2$ Gas Stocks with ^{15}N-Labeled Nitrate and Ammonium and Consequences for Nitrogen Fixation Measurements. *PLoS One* **2014**, *9*, No. e110335.
(22) Suryanto, B. H. R.; Du, H.-L.; Wang, D.; Chen, J.; Simonov, A. N.; MacFarlane, D. R. Challenges and Prospects in the Catalysis of Electroreduction of Nitrogen to Ammonia. *Nat. Catal.* **2019**, *2*, 290−296.
(23) Yao, Y.; Zhu, S.; Wang, H.; Li, H.; Shao, M. A Spectroscopic Study on the Nitrogen Electrochemical Reduction Reaction on Gold and Platinum Surfaces. *J. Am. Chem. Soc.* **2018**, *140*, 1496−1501.
(24) Yao, Y.; Wang, H.; Yuan, X.; Li, H.; Shao, M. Electrochemical Nitrogen Reduction Reaction on Ruthenium. *ACS Energy Lett.* **2019**, *4*, 1336−1341.
(25) Yao, Y.; Zhu, S.; Wang, H.; Li, H.; Shao, M. A Spectroscopic Study of Electrochemical Nitrogen and Nitrate Reduction on Rhodium Surfaces. *Angew. Chem. Int. Ed.* **2020**, *59*, 10479−10483.
(26) Liu, Y.; Wang, L.; Chen, L.; Wang, H.; Jadhav, A. R.; Yang, T.; Wang, Y.; Zhang, J.; Kumar, A.; Lee, J.; et al. Unveiling the Protonation Kinetics-Dependent Selectivity in Nitrogen Electroreduction: Achieving 75.05% Selectivity. *Angew. Chem. Int. Ed.* **2022**, *61*, No. e202209555.
(27) Zhang, L.; Zhou, H.; Yang, X.; Zhang, S.; Zhang, H.; Yang, X.; Su, X.; Zhang, J.; Lin, Z. Boosting Electroreduction Kinetics of Nitrogen to Ammonia via Atomically Dispersed Sn Protuberance. *Angew. Chem. Int. Ed.* **2023**, *62*, No. e202217473.
(28) Venturini, S. I.; Martins de Godoi, D. R.; Perez, J. Challenges in Electrocatalysis of Ammonia Oxidation on Platinum Surfaces: Discovering Reaction Pathways. *ACS Catal.* **2023**, *13*, 10835−10845.
(29) Lin, G.; Ju, Q.; Guo, X.; Zhao, W.; Adimi, S.; Ye, J.; Bi, Q.; Wang, J.; Yang, M.; Huang, F. Intrinsic Electron Localization of Metastable MoS_2 Boosts Electrocatalytic Nitrogen Reduction to Ammonia. *Adv. Mater.* **2021**, *33*, No. 2007509.
(30) Zhang, L.; Ji, X.; Ren, X.; Ma, Y.; Shi, X.; Tian, Z.; Asiri, A. M.; Chen, L.; Tang, B.; Sun, X. Electrochemical Ammonia Synthesis via Nitrogen Reduction Reaction on a MoS_2 Catalyst: Theoretical and Experimental Studies. *Adv. Mater.* **2018**, *30*, No. 1800191.
(31) Voiry, D.; Salehi, M.; Silva, R.; Fujita, T.; Chen, M.; Asefa, T.; Shenoy, V. B.; Eda, G.; Chhowalla, M. Conducting MoS_2 Nanosheets as Catalysts for Hydrogen Evolution Reaction. *Nano Lett.* **2013**, *13*, 6222−6227.
(32) Zhu, J.; Wang, Z.-C.; Dai, H.; Wang, Q.; Yang, R.; Yu, H.; Liao, M.; Zhang, J.; Chen, W.; Wei, Z.; et al. Boundary Activated Hydrogen Evolution Reaction on Monolayer MoS_2. *Nat. Commun.* **2019**, *10*, 1348.
(33) Xu, Y.; Ge, R.; Yang, J.; Li, J.; Li, S.; Li, Y.; Zhang, J.; Feng, J.; Liu, B.; Li, W. Molybdenum Disulfide (MoS_2)-Based Electrocatalysts for Hydrogen Evolution Reaction: From Mechanism to Manipulation. *J. Energy Chem.* **2022**, *74*, 45−71.
(34) Van Nguyen, T.; Tekalgne, M.; Nguyen, T. P.; Van Le, Q.; Ahn, S. H.; Kim, S. Y. Electrocatalysts Based on MoS_2 and WS_2 for Hydrogen Evolution Reaction: An Overview. *Battery Energy* **2023**, *2*, No. 20220057.
(35) Fujii, T.; Selvin, C. P.; Sablier, M.; Iwase, K. Analysis of Hydronitrogen Species Generated by a Microwave Discharge in (N_2H_4)/He. *J. Phys. Chem. A* **2002**, *106*, 3102−3105.
(36) Liu, Y.; Su, Y.; Quan, X.; Fan, X.; Chen, S.; Yu, H.; Zhao, H.; Zhang, Y.; Zhao, J. Facile Ammonia Synthesis from Electrocatalytic N_2 Reduction under Ambient Conditions on N-Doped Porous Carbon. *ACS Catal.* **2018**, *8*, 1186−1191.
(37) Chen, L.; Zhou, Y.; Rao, Y.; Qin, M.; Gong, B.; Zhang, W.; Li, Z. Improving the Nitrogen Reduction Reaction Performance of MoS_2 via a Synergetic Engineering Strategy. *Adv. Funct. Mater.* **2022**, *126*, No. 9352.
(38) Wang, J.; Nan, H.; Tian, Y.; Chu, K. $FeMo_3S_4$ for Efficient Nitrogen Reduction Reaction. *ACS Sustain. Chem. Eng.* **2020**, *8*, 12733−12740.
(39) Watt, G.; Chrisp, J. A Spectrophotometric Method for the Determination of Hydrazine. *Anal. Chem.* **1952**, *24*, 2006−2008.

(40) Foner, S.; Hudson, R. Diimide - Identification and Study by Mass Spectrometry. *J. Chem. Phys.* **1958**, *28*, 719−720.
(41) Chu, K.; Liu, Y.-P.; Li, Y.-B.; Wang, J.; Zhang, H. Electronically Coupled SnO_2 Quantum Dots and Graphene for Efficient Nitrogen Reduction Reaction. *ACS Appl. Mater. Interfaces* **2019**, *11*, 31806−31815.
(42) Wu, L.; Ji, Y.; Dai, D.; Chen, T.; Yang, D.; Liu, Y.; Wang, Z. Exceptional Size-Dependent Activity Enhancement in the Catalytic Electroreduction of N_2 over Mo Nanoparticles. *Int. J. Hydrogen Energy* **2020**, *45*, 31841−31848.
(43) Li, X.; Ren, X.; Liu, X.; Zhao, J.; Sun, X.; Zhang, Y.; Kuang, X.; Yan, T.; Wei, Q.; Wu, D. A MoS_2 Nanosheet−Reduced Graphene Oxide Hybrid: An Efficient Electrocatalyst for Electrocatalytic N_2 Reduction to NH_3 under Ambient Conditions. *J. Mater. Chem. A* **2019**, *7*, 2524−2528.

https://doi.org/10.1021/acselectrochem.4c00135
ACS Electrochem. 2025, 1, 294−302